A Parameterization of Shear-Driven Turbulence for Ocean Climate Models

L. JACKSON

Atmospheric and Oceanic Sciences, Princeton University, Princeton, New Jersey

R. HALLBERG

Geophysical Fluid Dynamics Laboratory, Princeton, New Jersey

S. LEGG

Atmospheric and Oceanic Sciences, Princeton University, Princeton, New Jersey

(Manuscript received 14 February 2007, in final form 14 September 2007)

ABSTRACT

This paper presents a new parameterization for shear-driven, stratified, turbulent mixing that is pertinent to climate models, in particular the shear-driven mixing in overflows and the Equatorial Undercurrent. This parameterization satisfies a critical requirement for climate applications by being simple enough to be implemented implicitly and thereby allowing the parameterization to be used with time steps that are long compared to both the time scale on which the turbulence evolves and the time scale with which it alters the large-scale ocean state.

The mixing is expressed in terms of a turbulent diffusivity that is dependent on the shear forcing and a length scale that is the minimum of the width of the low Richardson number region ($\mathrm{Ri} = N^2/|\mathbf{u}_z|^2$, where N is the buoyancy frequency and $|\mathbf{u}_z|$ is the vertical shear) and the buoyancy length scale over which the turbulence decays [$L_b = Q^{1/2}/N$, where Q is the turbulent kinetic energy (TKE)]. This also allows a decay of turbulence vertically away from the low Richardson number region over the buoyancy scale, a process that the results show is important for mixing across a jet. The diffusivity is determined by solving a vertically nonlocal steady-state TKE equation and a vertically elliptic equilibrium equation for the diffusivity itself.

High-resolution nonhydrostatic simulations of shear-driven stratified mixing are conducted in both a shear layer and a jet. The results of these simulations support the theory presented and are used, together with discussions of various limits and reviews of previous work, to constrain parameters.

1. Introduction

Although shear-driven turbulence in the ocean occurs over small scales, there are regions where the influence of this mixing can have a large-scale impact. In particular, the shear-driven mixing in both the Equatorial Undercurrent (EUC) and in overflows is climatically significant. In the former case, it is clear that mixing in the EUC affects the sea surface properties and hence has a direct influence on the climate. Mixing in overflows, despite the fact that it occurs well below the ocean surface, can still significantly impact the climate. The overflows in the North Atlantic, the Denmark Straits overflow, and the Faroe Bank Channel overflow together supply most of the North Atlantic Deep Water, which forms the dominant water mass of the deep branch of the thermohaline circulation. Similarly, the overflows from the Antarctic shelf are the source of Antarctic Bottom Water. Mixing between the dense overflow water and the overlying water reduces the density and increases the volume of the deep water. To understand and predict how the Atlantic's overturning circulation may evolve in alternative climate regimes, and how this in turn may provide feedbacks on the climate, it is necessary to predict how much mixing occurs in these overflows and where the mixing is located. Although the overflow mixing is localized, it can have a profound influence on the large-scale circulation by modifying properties and transports of deep water masses, which in turn can influence overlying currents.

Corresponding author address: Dr. L. Jackson, GFDL, Forrestal Campus, Route 1, Princeton, NJ 08542.
E-mail: laura.jackson@noaa.gov

DOI: 10.1175/2007JPO3779.1

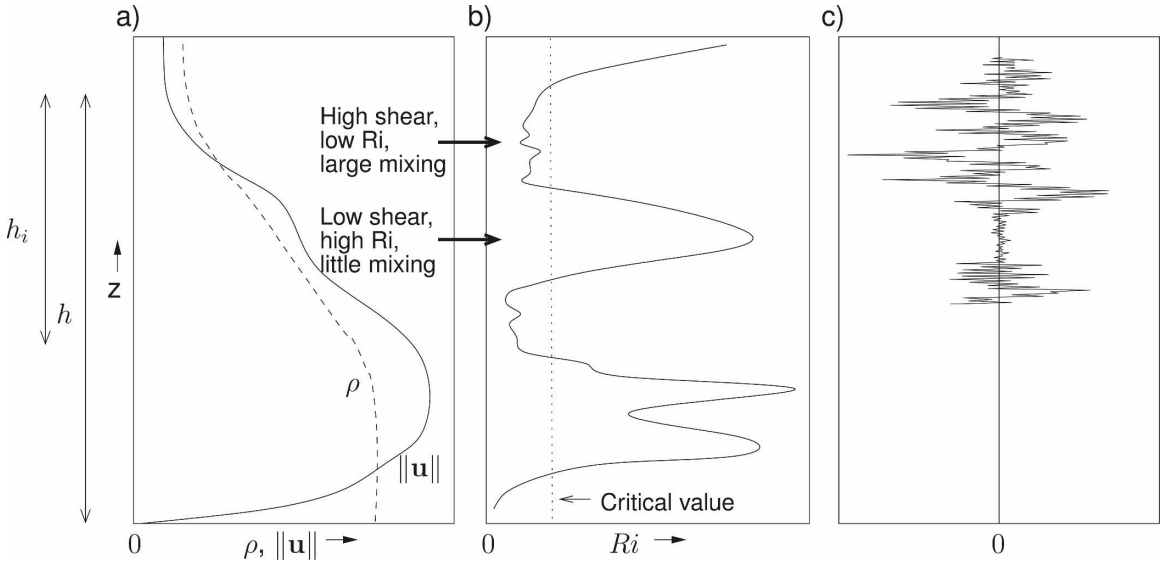

FIG. 1. Schematic of an overflow plume: vertical profiles of (a) speed (solid line) and density (dashed line), (b) Richardson number, and (c) vertical turbulent displacement. Note that where the velocity shear is large, the Richardson number is less than its critical value and there is vigorous mixing, whereas where the shear is small and the Richardson number large there is little mixing. Source for schematic is data from the Red Sea outflow plume in Peters and Johns (2005); the bottom part of (c) is blank because of missing data in Peters and Johns (2005).

For example, in an isopycnal model (in which there is minimal numerical diapycnal mixing), when parameterized mixing is removed from the Nordic overflows, sea surface temperature differences of a few degrees are produced in the North Atlantic on a time scale of only a few years.

Although the circumstances leading to mixing in overflows and in the EUC are very different, the main mixing process in both cases is due to shear-driven stratified turbulence. In an overflow the gravitational acceleration of dense fluid flowing down topographical slopes creates a velocity shear at the interface between the dense fluid and overlying ambient water. When the gradient Richardson number is sufficiently small, this shear generates instabilities and turbulence. Figure 1 shows a schematic of vertical profiles in the Red Sea outflow based on data from Peters and Johns (2005). At the top of the gravity current there are regions with large shear and low Richardson number (Ri) that exhibit overturns due to turbulent mixing as seen in the vertical turbulent displacement. These characteristics suggest that a shear-driven mixing parameterization would be appropriate at the top of the plume. There is also a region at the base of the plume with low Ri due to large shear caused by frictional drag on the ocean floor (even though it is the shear at the top of the plume that is driving the entrainment into the plume). This bottom boundary layer process has been credibly parameterized in Legg et al. (2006) by assuming that 20% of the energy removed by bottom drag is used to homogenize a turbulent bottom boundary layer.

In the EUC the flow is driven by a horizontal pressure gradient generated by equatorial trade winds. The structure of the current creates velocity shears at the top and bottom of the jet, driving turbulent mixing where the Richardson number is low. If the mixing in both overflows and the EUC is simply due to shear-driven turbulence, then we would expect a parameterization of this process to capture the mixing in both scenarios. Chang et al. (2005) compared the entrainment predicted by the interior part of the *K*-profile parameterization (KPP)—that is, parameterizing the shear-driven mixing in the Pacific EUC—to large-eddy simulations (LES) of gravity currents and found that the magnitude of the mixing had to be increased by a factor of 50 to fit the data. Since this parameterization involves dimensional constants that have been calibrated for the Pacific EUC, it is not surprising that it does not work in a different regime where the length scales and velocity shears driving the turbulence are different. It has also been shown in global ocean simulations with the Hallberg Isopycnal Model (HIM) that neither the interior part of KPP nor the Hallberg (2000) parameterization can be tuned to give reasonable mixing for both the EUC and overflows: either the EUC is much too diffuse or the Mediterranean overflow (for example) is much too deep. This inconsistency highlights the need for an improved parameterization; how-

ever, any such parameterization must be relatively simple to be useful for a climate model. Since a climate model typically requires time steps that are long compared to the time scales of the turbulence, the mixing must be treated implicitly, and hence the parameterization should be sufficiently simple to be implemented in this way.

Perhaps the most difficult issue in constructing a parameterization that is simple enough to be used for climate models is how to represent the turbulent length scales. The interior part of KPP and similar parameterizations simply use a prescribed dimensional length, whereas the Hallberg (2000) parameterization uses the vertical extent of the low Richardson number region. All these parameterizations assume that turbulent mixing stops once the Richardson number reaches a critical value; however, we will demonstrate that the turbulence can penetrate vertically away from the low Richardson number region. Hence we base our parameterization on two vertical length scales: the vertical extent of the low Richardson number region, and the buoyancy length scale (the length scale over which the turbulent velocity fluctuations are affected by stratification). To assess the importance of this vertical propagation, we investigate the mixing in a jet, where the Richardson number becomes large in the core, as well as in a shear layer.

In the following sections we discuss current parameterizations in geopotential and isopycnal models, the ways in which these are linked, and the implications for general parameterizations. We then proceed to outline our new parameterization and discuss how it compares to well-understood limits. Sets of parameters are found by studying previous research and comparing our parameterization to high-resolution nonhydrostatic simulations of shear-driven stratified turbulent mixing in shear and jet flow. Our parameterization reproduces the salient features of these simulations and performs well compared with other parameterizations. We then discuss how this parameterization is implemented in ocean climate models.

2. Existing parameterizations

There are several parameterizations currently used for predicting shear-driven mixing. In geopotential models this turbulent mixing is generally expressed as a diffusion of density due to an eddy diffusivity κ such that

$$D\rho/Dt = \partial(\kappa\partial\rho/\partial z)/\partial z$$

where

$$D\rho/Dt = d\rho/dt + \mathbf{u}\cdot\nabla\rho. \tag{1}$$

This diffusivity is often expressed in terms of a gradient Richardson number $\mathrm{Ri} = N^2/S^2$, where S is the vertical shear ($S = ||\mathbf{u}_z||$) and N is the buoyancy frequency ($N^2 = -g\rho_z/\rho_o$). One commonly used parameterization is the interior part of KPP (Large et al. 1994), where κ is given by

$$\kappa = \kappa_o\left[1 - \min\left(1, \frac{\mathrm{Ri}}{\mathrm{Ri}_c}\right)^2\right]^3, \tag{2}$$

with $\kappa_o = 5\times10^{-3}\ \mathrm{m^2\,s^{-1}}$ and $\mathrm{Ri}_c = 0.7$. Although this has been calibrated for the Pacific EUC, the dimensional constant κ_o implies that this cannot be a universal parameterization, since the magnitude of the diffusion is not dependent on the length and time scales of the flow. Therefore there is no reason to expect that this parameterization would be appropriate for overflows. Parameterizations such as this are local in the sense that the diffusivity is only dependent on the local gradient Richardson number. Other similar local parameterizations include Pacanowski and Philander (1981) and Yu and Schopf (1997), which are also subject to the same criticisms as the interior part of KPP. There are also more complex models to predict the eddy diffusivity, such as two equation turbulence models, which will be discussed in section 5d.

Isopycnal coordinates are the natural coordinate system for simulating shear-driven mixing of density since the resolution naturally concentrates in regions of high stratification. There is also no numerical mixing across density surfaces, so all diapycnal mixing is specified as a change of layer thickness given by

$$\frac{\partial}{\partial t}\left(-\frac{\partial z}{\partial\rho}\right) + \nabla\cdot\left(-\frac{\partial z}{\partial\rho}\mathbf{u}\right) = \frac{\partial w^*}{\partial\rho}, \tag{3}$$

where w^* is the cross-diapycnal velocity (McDougall and Dewar 1998). Hallberg (2000) parameterized the turbulent entrainment into gravity currents by expressing the right-hand side of this as

$$\frac{\partial w^*}{\partial\rho} = 2\left\|\frac{\partial\mathbf{u}}{\partial\rho}\right\|F(\mathrm{Ri}). \tag{4}$$

The function $F(\mathrm{Ri})$ is a function of the Richardson number given by $\max\{0.08\,[(1 - \mathrm{Ri}/\mathrm{Ri}_c)/(1 + 5\mathrm{Ri})], 0\}$, with a critical Richardson number of $\mathrm{Ri}_c = 0.8$. This parameterization uses interior "boundary conditions" such that ω^* reverts to a background diffusive value $w^* = \partial(\kappa_\theta\partial\rho/\partial z)/\partial\rho$ with the background diffusivity κ_o wherever $\mathrm{Ri} > \mathrm{Ri}_c$. This is generally referred to as the Turner parameterization (TP) since it is based on the laboratory studies of Ellison and Turner (1959) and Turner (1986). In those studies the increase in thickness h of the entraining gravity current was found to depend both on the velocity difference ΔU between the gravity current and the ambient fluid and on the bulk Richard-

son number $\mathrm{Ri}_b = (g\Delta\rho h)/(\rho_o \Delta U^2)$ (where $\Delta\rho$ is the density difference between the dense current and the ambient water). This is similar to the gradient Richardson number except it is dependent on the bulk properties of the system rather than local gradients. Since the formulation used in Hallberg (2000) is for the change in layer thickness due to the gradient Richardson number rather than the bulk Richardson number, it is not clear that this parameterization is directly transferable. Papadakis et al. (2003) examined the sensitivity of this parameterization to the entrainment rate and the critical value of Ri below which mixing stops, and found that the latter is the most important in modifying water mass properties in the Mediterranean outflow. A modified version of this parameterization is developed by Xu et al. (2006), who use a linear function of $F(\mathrm{Ri})$ to compare against nonhydrostatic LES of gravity currents. They find the best fit to their data is with the form $F(\mathrm{Ri}) = \max[0.2(1-\mathrm{Ri}/0.25), 0]$, although their solution is not very sensitive to the entrainment rate. An interesting point to note is that the critical value in this case is 0.25, which is the critical value predicted by linear instability analysis for the growth of Kelvin–Helmholtz (KH) instabilities in a shear layer (Miles 1961).

Since there are parameterizations in both isopycnal and geopotential coordinate systems, it is illuminating to consider how these are linked. We can compare parameterizations in both coordinate systems by expressing the diapycnal velocity in (3) in terms of the Lagrangian change of density $w^* = (\partial z/\partial\rho)(D\rho/Dt)$. Then, using the diffusive closure of (1), we can calculate an equivalent eddy diffusivity for the change of layer thickness in isopycnal coordinates, giving

$$\frac{\partial}{\partial t}\left(-\frac{\partial z}{\partial \rho}\right) + \boldsymbol{\nabla}\cdot\left(-\frac{\partial z}{\partial \rho}\mathbf{u}\right) = \frac{1}{\rho_z}\frac{\partial}{\partial z}\left[\frac{1}{\rho_z}\frac{\partial}{\partial z}(\kappa\rho_z)\right]. \tag{5}$$

Parameterizing the right hand side of this as in Hallberg (2000) [see (4)] implies an equivalent eddy diffusivity for geopotential coordinates given by the solution of

$$\frac{\partial}{\partial z}\left[\frac{1}{\rho_z}\frac{\partial}{\partial z}(\kappa\rho_z)\right] = -2SF(\mathrm{Ri}), \tag{6}$$

where S is the vertical shear ($S = \|\mathbf{u}_z\|$) and we have assumed stable stratification. The boundary conditions are that (6) is valid for $\mathrm{Ri} \le \mathrm{Ri}_c$ with $\kappa = 0$ for $\mathrm{Ri} > \mathrm{Ri}_c$. There are issues with this parameterization in that where the stratification is zero the eddy diffusivity is not well defined. Although this is not a problem in isopycnal coordinates since there is always, in practice, a nonzero stratification due to the definition of layers, it makes this parameterization difficult to apply to geopotential coordinate models, particularly if the turbulent eddy diffusivity is used to mix momentum or a tracer. The main issue with this parameterization, however, is that it assumes that a parameterization for the bulk entrainment into a plume based on the bulk properties of the plume can be directly applied to the entrainment into an isopycnal layer according to the local vertical gradients of velocity and density. This approach ignores any internal structure to the mixing.

The observations underpinning TP are applicable to the change in layer thickness integrated over the entire turbulent layer, rather than for individual layers. This would imply that

$$\frac{\partial h}{\partial t} + \boldsymbol{\nabla}\cdot\mathbf{U} = -\left(\frac{\partial \kappa}{\partial z} + \kappa\frac{\rho_{zz}}{\rho_z}\right)\bigg|_{\text{top of plume}}, \tag{7}$$

where $h = \int_{\rho_t}^{\rho_b} -z_\rho d\rho$ and $\mathbf{U} = \int_{\rho_t}^{\rho_b} -z_\rho \mathbf{u} d\rho$; and ρ_b and ρ_t are the density at the top and bottom of the plume, respectively. Here we have taken the density at the top of the plume to be fixed by definition, and defined the bottom of the plume (with $\mathbf{u}_b = 0$) by the topography. The entrainment into the plume occurs at the top of the plume because of a mixing layer of width h_i (see Fig. 1). If we make the assumption that the stratification and shear over this mixing layer are constant, then Ri is constant and (6) gives κ via

$$\frac{\partial^2 \kappa}{\partial z^2} = -2SF(\mathrm{Ri}) \tag{8}$$

over the mixing region where $\mathrm{Ri} < \mathrm{Ri}_c$, and $\kappa = 0$ outside it. Since κ is also symmetric about the center of the layer, integrating across the layer gives $(\partial\kappa/\partial z)|_{\text{top of plume}} = -\Delta U F(\mathrm{Ri})$. Note that the factor of 2 appears in our parameterization since there is entrainment at the top and bottom of each layer, though with the assumptions here these are equal. Comparing with (7), we find the increase in layer thickness is given by

$$\frac{\partial h}{\partial t} + \boldsymbol{\nabla}\cdot\mathbf{U} = \Delta U F(\mathrm{Ri}) \tag{9}$$

since we have assumed $\kappa = 0$ at the top of the plume. This is similar to the relationship found in the laboratory results of Turner (1986), in that the entrainment is related both to the velocity difference between the dense plume and overlying water and to a nondimensional factor that is dependent on a Richardson number. Note, however, that $\mathrm{Ri} \neq \mathrm{Ri}_b$; in fact, $\mathrm{Ri} = \mathrm{Ri}_b h_i/h < \mathrm{Ri}_b$, implying that the function $F(\mathrm{Ri})$ of the gradient Richardson number should not be the same function as that found in TP for the bulk Richardson

number. In particular, the critical Richardson number [where $F(\mathrm{Ri}) = 0$] should be smaller than in TP.

Although this parameterization compares well with these laboratory results it is still essentially a local parameterization on account of the interior "boundary conditions." There is mixing in the low Richardson number region, but this can never spread outside the region, and there can never be mixing in regions of zero shear. We will demonstrate that this is not always the case, especially for a jet where there can be mixing across the zero shear in the center of the jet. Indeed this can also be seen in the direct numerical simulation (DNS) studies of Tse et al. (2003). Another problem with local parameterizations is that a small change in Ri from above to below the critical value can produce a large change in the magnitude of the mixing. For this parameterization in particular this also dramatically affects the magnitude of the mixing in nearby regions, since $\kappa \sim SL^2$, where L is the width of the of the low Richardson number region. It seems desirable to have a parameterization that changes more smoothly from one regime to another and allows a vertical transport of turbulence away from the mixing region.

3. New parameterization

Having considered the implications of associating TP with a turbulent eddy diffusivity above, we propose a new parameterization for the eddy diffusivity in shear-driven stratified turbulence given by

$$\frac{\partial^2 \kappa}{\partial z^2} - \frac{\kappa}{L_d^2} = -2SF(\mathrm{Ri}). \tag{10}$$

This is similar to the locally constant stratification limit of TP (8), but with the addition of a decay length scale $L_d = \lambda L_b$. Here $L_b = Q^{1/2}/N$ is the buoyancy length scale where Q is the turbulent kinetic energy (TKE) per unit mass, and λ is a nondimensional constant that will be discussed in section 4c. The function $F(\mathrm{Ri})$ is a function of the Richardson number that remains to be determined, and may be different in form from that in TP, although there must be a critical value of Ri above which $F(\mathrm{Ri}) = 0$. There are then two length scales: the width of the low Richardson number region as before [from the first term in (10)], and the buoyancy length scale, which is the length scale over which the TKE is affected by the stratification (see appendix A for a more detailed discussion of the length scales). In particular, the inclusion of a decay length scale means that the diffusivity decays exponentially away from the mixing region with a length scale of L_d. This is important since turbulent eddies generated in the low Ri layer can be vertically self-advected and mix nearby regions. In addition to its physical importance, which we will discuss more below, this method also yields a smoother diffusivity than the Hallberg (2000) scheme, especially in areas where the Richardson number is noisy.

Our parameterization predicts the turbulent eddy diffusivity in terms of the vertical profiles of velocity and density, providing that the TKE is known. To complete our parameterization we use a TKE Q budget such as that used in second-order turbulence closure models (see Umlauf and Burchard 2005). We make a few additional assumptions, however, and use the simplified form

$$\frac{\partial}{\partial z}\left[(\kappa + \nu_o)\frac{\partial Q}{\partial z}\right] + \kappa(S^2 - N^2) - Q(c_N N + c_S S) = 0. \tag{11}$$

The system is therefore in balance between a vertical diffusion of TKE caused by both the eddy and molecular viscosity (ν_0), the production of TKE by shear, a sink due to stratification, and the dissipation. Note that we are assuming a Prandtl number of 1, although a parameterization for the Prandtl number could be added. We have assumed that the TKE reaches a quasi-steady state faster than the flow is evolving and faster than it can be affected by mean-flow advection so that $DQ/Dt = 0$. Since this parameterization is to be used in climate models with low horizontal resolution and large time steps compared to the mixing time scales, this is a reasonable assumption. Our most tenuous assumption is in the form of the dissipation $\varepsilon = Q(c_N N + c_S S)$ (where c_N and c_S are parameters to be determined), which is assumed to be dependent on the buoyancy frequency (through loss of energy to internal waves) and the velocity shear (through the energy cascade to smaller scales; see Shih et al. 2000). This can also be written as $\varepsilon = Q^{3/2}(c_N/L_b + c_S/L_s)$ so that the dominant length scale for the dissipation is the minimum of the buoyancy length scale and the shear length scale, $L_s = Q^{1/2}/S$. This budget is for kinetic energy caused by 3D turbulence only, rather than that caused by internal waves, since the waves do not necessarily contribute to mixing. Hence it is difficult to compare TKE balances with laboratory or oceanic data since these generally include internal wave effects.

It is worth observing that our equation for diffusivity Eq. (10) is equivalent to a steady "transport" equation for the turbulent diffusivity (i.e., with $D\kappa/Dt = 0$),

$$\frac{\partial}{\partial z}\left(\kappa\frac{\partial \kappa}{\partial z}\right) + 2\kappa SF(\mathrm{Ri}) - \left(\frac{\kappa}{L_d}\right)^2 - \left(\frac{\partial \kappa}{\partial z}\right)^2 = 0,$$

as noted by Lars Umlauf (L. Umlauf 2007, personal communication). The first term on the left can be re-

garded as a vertical transport of diffusivity, the second term as a source, and the final two as sinks. Using this as a second equation (along with that for the TKE) has an advantage over standard two equation turbulence models such as κ–ε and Mellor–Yamada (see section 5d) because the eddy diffusivity being prescribed is calculated directly and these equations are simple enough to solve quickly using an iterative technique.

We also need boundary conditions for (10) and (11). For the turbulent diffusivity we use $\kappa = 0$ since our diffusivity is numerically defined on layer interfaces. This ensures that there is no turbulent flux across boundaries. If the diffusivity is instead defined within a layer then an alternative based on the logarithmic layer of the wall should be used (see Burchard et al. 2005). For the TKE we use boundary conditions of $Q = Q_0$ where Q_0 is a constant value of TKE, used to prevent a singularity in (10), that is chosen to be small enough to not influence results. Note that the value of κ calculated here reflects shear-driven turbulent mixing only; the total diffusivity would be this value plus any diffusivities due to other turbulent processes (e.g., internal wave-driven mixing, convection, mechanically forced boundary turbulence) or a background value.

In the following sections we assess our parameterization in various well-understood limits to verify that it behaves well in these limits and is consistent with established research.

a. Homogeneous stratified turbulence

One limit that has been widely studied is the limit of homogeneous turbulence where vertically uniform profiles of shear and stratification are maintained in an infinite domain (Baumert and Peters 2000). In this limit our system predicts that $\kappa \propto S\, L_b^2$ and gives a relationship for Ri as follows:

$$2\lambda^2 F(\mathrm{Ri}) = \frac{\mathrm{Ri}(c_N \mathrm{Ri}^{1/2} + c_S)}{1 - \mathrm{Ri}}. \tag{12}$$

The function $F(\mathrm{Ri})$ is as yet unknown; however, it decreases from a positive value F_o at Ri = 0 to zero at a critical value of Ri, and hence the left-hand side decreases monotonically to zero at $\mathrm{Ri} = \mathrm{Ri}_c$. The right-hand side increases monotonically from zero and becomes singular at Ri = 1, which is expected to be greater than the critical value. Hence there is a unique value of $\mathrm{Ri} < \mathrm{Ri}_c$ for which this equation holds and where homogeneous turbulence is possible. In general Ri is not only different from this value, but varies with depth, in which case all other steady-state solutions must have a nonlocal balance.

In homogeneous turbulence studies, full equilibrium (where the turbulent properties do not vary with time) is only achieved for a single flux Richardson number ($\mathrm{Ri}_f = \mathrm{Ri}/\sigma$, where σ is the turbulent Prandtl number) and gradient Richardson number (see Burchard and Baumert 1995). Various laboratory and DNS results suggest values for this steady-state Richardson number of 0.2–0.25 at high Reynolds numbers (Rohr et al. 1988; Shih et al. 2000), with two equation turbulence models using values of 0.2–0.3 (Umlauf and Burchard 2005).

b. Unstratified limit

The second limit we consider is that of an unstratified shear flow. Since we are assuming a turbulent Prandtl number of 1 we can calculate the viscosity from (10) giving

$$\frac{\partial^2 \nu}{\partial z^2} = -2F_o \left| \frac{\partial u}{\partial z} \right|, \tag{13}$$

where $F_o = F(0)$, and we use $\nu = \kappa$ to represent the eddy viscosity (with boundary conditions of $\nu = 0$ at the boundaries).

One well-verified characteristic of unstratified turbulent shear flow is the law of the wall (Lesieur 1997; Moin and Kim 1982). This predicts that near a solid boundary where the stress is constant, the eddy viscosity linearly increases away from the boundary and the velocity increases in a log-layer. With a large velocity shear near the boundary, however, our parameterization is inconsistent with a linearly varying viscosity. To reconcile our parameterization with this well-tested theory, we modify our parameterization to set $L_d = \min(\lambda L_b, L_z)$ in (10), where L_z is the distance to the nearest solid boundary. This can be understood by considering L_d to be the size of the largest turbulent eddies, whether they are constrained by the stratification (through L_b) or through the geometry (through L_z).

A channel flow with constant stress satisfies $\nu|u_z| = u^{*2}$ in equilibrium (see Lesieur 1997, 114–119), where $u^* = \sqrt{\tau_o/\rho_o}$ is the stress velocity with surface stress τ_o. This then allows our new parameterization for the unstratified case to be

$$\frac{\partial^2 \nu}{\partial z^2} - \frac{\nu}{L_z^2} = -\frac{2F_o u^{*2}}{\nu}. \tag{14}$$

The numerical solution to (14) between two solid boundaries with a constant stress (Couette flow) is plotted in Fig. 2, where we have taken L_z to be half the harmonic mean of the distance to both boundaries, where the total width is D. This means that $L_z = [z(D - z)]/D$ asymptotically approaches the distance to a relatively close boundary. The predicted viscosity is then approximately parabolic with $\nu \approx \sqrt{2F_o} u^* L_z =$

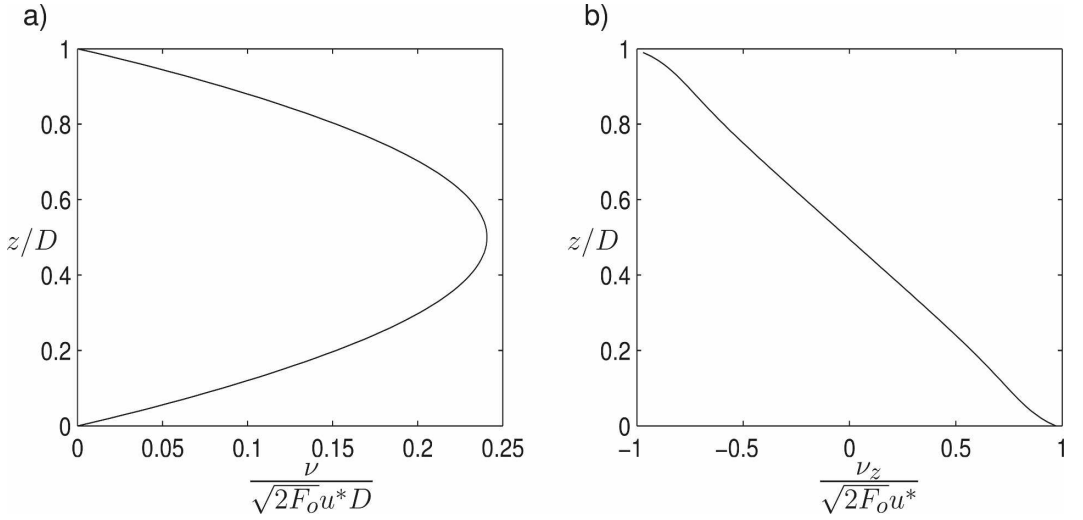

FIG. 2. (a) Eddy viscosity and (b) its gradient for Couette flow (unstratified flow in a channel with a constant stress) as predicted by our parameterization using L_z as half the harmonic mean of the distances to each boundary.

$\sqrt{2F_o}u^*[z(D-z)]/D$, giving $(\partial\nu/\partial z)|_{z=\pm1} \approx \pm\sqrt{2F_o}u^*$. This satisfies the law of the wall providing that $F_o \approx 0.084$, which gives a von Kármán constant of 0.41.

In summary, our parameterization is consistent both with the Turner (1986) results for gravity currents under appropriate assumptions and with the homogeneous stratified turbulence literature. In the unstratified limit we can slightly modify our parameterization for use near boundaries where we can recover the law of the wall.

4. Constraining parameters

We have shown that our new parameterization gives reasonable results in the limits discussed; however, for our theory to be complete, there are several parameters that must be given. These are the critical Richardson number Ri_c, the magnitude and shape of the mixing function $F(\mathrm{Ri})$, and the length scale ratio $\lambda = L_d/L_b$ from (10). Also the two dissipation parameters c_N and c_S from (11) must be found. Although these will be determined in section 5 by comparisons with model results, we can constrain most of these parameters by referring to previous studies of turbulent mixing. Appropriate parameter ranges are shown in Table 1.

a. Form of F(Ri)

Following TP we use the monotonically decreasing function

$$F(\mathrm{Ri}) = F_o\left(\frac{1-\mathrm{Ri}/\mathrm{Ri}_c}{1+\alpha\mathrm{Ri}/\mathrm{Ri}_c}\right),$$

where α is the curvature parameter. We require $\alpha > -1$, but there is no other a priori restriction on the shape. The two important properties of $F(\mathrm{Ri})$ are the critical Richardson number at which $F(\mathrm{Ri}) = 0$ for $\mathrm{Ri} \geq \mathrm{Ri}_c$ (which will be discussed in the following section) and the magnitude of mixing $F_o = F(0)$.

Turner (1986) chose a value of $F_o = 0.08$ to fit his data after studying previous experiments of unstratified mixing in jets and plumes, which found values ranging from $F_o = 0.07$–0.22 based on a layer growth defined by a velocity profile. For our modified parameterization (as described in section 3b) to be consistent with the law of the wall, we require a von Kármán constant of $\approx$0.41 and hence a value of $F_o \approx 0.084$. Therefore, we want a value of F_o close to 0.08.

b. Critical Richardson number

The existence of a critical Richardson number above which turbulent mixing does not occur was first suggested by Miles (1961), who showed that $\mathrm{Ri} > 1/4$ is a sufficient condition for the stability of stratified shear flows in exponentially growing modes. Flows with smaller Richardson numbers are subject to the KH instability mechanism where instabilities can grow and roll up into KH billows. Secondary instabilities then lead to degeneration into three-dimensional turbulent mixing. Some mixing can also be generated by Hölm-

TABLE 1. Parameter ranges from previous work.

Parameter	Range
Ri_c	0.25–0.35
F_o	$\approx$0.084
λ	$O(1)$
c_N, c_S	0.1–1.0

böe instabilities at larger gradient Richardson numbers (Strang and Fernando 2001), although this mixing is substantially weaker than that generated by KH instabilities. There have also been suggestions that the critical Richardson number could be as large as 1 based on nonlinear stability arguments (Abarbanel et al. 1986).

Some numerical DNS results (Smyth and Moum 2000) and laboratory results (Koop and Browand 1979) have suggested a slightly higher value of ~0.3, and others a value as high as ~1 (Strang and Fernando 2001). The method of calculation can play a large role—for instance, a global Ri based on the minimum value in a column will generally be much lower than an average value, and also more indicative of the turbulent state. In the same way, calculating Ri based on time and spatial averages of the stratification and velocity shear at fixed depths may indicate the presence of mixing at values greater than the critical value. For oceanographic data there are additional issues. Insufficient vertical resolution could lead to a spuriously large value of Ri (see Peters et al. 1995b) when the vertical gradients are not resolved, though De Silva et al. (1999) show that the sampled Ri does not change with resolution, provided that the vertical distance between samples is less than the Ozmidov scale. Another important issue with oceanographic profiles is that they are generally instantaneous, so the values of Ri measured may not be those that generated the turbulence; in particular, turbulence may be decaying in time or space.

Values of Ri_c used in parameterizations are also varied. TP and the interior part of KPP both use high values of 0.8 and 0.7 respectively, though the former is based on a bulk, rather than gradient, Richardson number. The more recent results of Xu et al. (2006) show that a critical value of 0.25 gives good agreement with LES results of gravity currents. Second-order turbulence closure models use various values ranging from 0.2 to 1.0; however, their definition of a critical Richardson number is for the complete extinction of turbulence in models assuming full equilibrium. A better comparison may be with the steady-state Richardson number Ri_s, since turbulence decays exponentially for $\mathrm{Ri} > \mathrm{Ri}_s$ (Umlauf et al. 2003). We would expect our Ri_c to be a bit larger than the steady-state values of 0.2–0.3 found in DNS and laboratory experiments (see section 3a for references), hence for our parameterization we suggest a value in the range of $\mathrm{Ri}_c \sim 0.25$–0.35.

c. Length scales

The first parameter introduced is $\lambda = L_d/L_b$, the ratio between a turbulent decay scale over which the diffusivity decays and the buoyancy length scale L_b. There are many different, but related, length scales discussed in the literature, the most common being the Thorpe scale (L_T), the Ellison scale (L_E), the Ozmidov scale (L_{oz}), and the buoyancy scale (L_b). The Thorpe length scale is calculated by reordering potential density profiles to produce equivalent stable profiles, with L_T then equal to the displacement due to the reordering. This is unaffected by nonoverturning internal waves and is a good measure when there is a single overturn, but can be more complicated if there are interacting overturns. The Ellison scale is given by $L_E = \rho'/\rho_z$ (where ρ' is the RMS fluctuation of the density about its mean) and is generally well correlated with L_T (Moum 1996; Smyth and Moum 2000). The influence of the stratification on the turbulent eddies is measured by the Ozmidov scale ($L_{\mathrm{oz}} = \sqrt{\varepsilon/N^3}$), which is the smallest length scale to be affected by the stratification. The buoyancy length scale is also a measure of the influence of buoyancy on the small-scale motions, although L_b is also influenced by internal waves included in Q. Note that much of the previous literature defines the buoyancy length scale as q/N, where $q = \sqrt{2Q}$ is a typical turbulence velocity scale.

While it remains unclear what length scale controls the decay of diffusivity away from the low Ri region, we parameterize this length scale as $L_d = \lambda L_b$. The buoyancy length scale diagnosed from our model results is affected by internal waves that do not necessarily mix; however, neither the Ellison nor the Ozmidov scale is suitable for our parameterization since each requires details of subgrid-scale density structure, and the Ozmidov length scale lacks a suitable parameterization for the dissipation. The buoyancy length scale is a more viable alternative since the TKE balance is based on physical principles, although assumptions must be made in the closures.

Various studies of the relationships between these length scales have shown that they are all related to some extent. Moum (1996) finds the relationships $L_E \approx 0.6L_T \approx 0.7L_{\mathrm{oz}} \approx 0.6L_b$, where the length scales are the RMS values taken from data studies in the ocean thermocline. However, these ratios vary from study to study. The DNS studies of Smyth and Moum (2000) indicate a smaller value of about $L_b/L_T \approx 0.6$ rather than 1, and the data study of Peters et al. (1995a) suggests a value of 1.6 from local length scales, although there is a lot of scatter. The way in which these length scales are calculated may play a large role: Peters et al. (1995a) find no correlation between instantaneous values of L_{oz} and L_T. However, when the same data are time averaged at constant depths the relationship then matches well with $L_{\mathrm{oz}} \approx 0.8L_T$ from Dillon (1982), which is found by carefully averaging properties over turbulent events. It has also been shown that these ra-

tios can evolve in time from a mixing event (L_{oz}/L_T can indicate the age of turbulent mixing; Smyth and Moum 2000) and can depend on the Richardson number (Baumert and Peters 2000). The length scales can also vary significantly in depth when the turbulent mixing is not homogeneous. Tse et al. (2003) and Joseph et al. (2004) calculate average length scales as a function of depth from quasi-steady turbulent mixing in a stratified jet, and although L_E is relatively constant across the domain, the Ozmidov and buoyancy length scales vary by two orders of magnitude. However, the ratio L_{oz}/L_b remains approximately 1 over the center of the jet, and then decreases away from the jet where there is a greater influence of inertial waves.

This review indicates that while these different length scales are not equivalent, they are certainly related and are of the same order of magnitude. Hence we take $\lambda = O(1)$.

d. Dissipation parameters

The ratio of L_{oz}/L_b also gives an indication of the parameters c_N and c_S since

$$2\left(\frac{L_{oz}}{L_b}\right)^2 = \frac{\varepsilon}{QN} = c_N + c_S \mathrm{Ri}^{-1/2}. \tag{15}$$

Moum (1996) finds the relationship $\varepsilon \approx 0.73w^2N$ where w is the rms vertical velocity fluctuation. Assuming isotropic turbulence this would give $\varepsilon/QN = 0.49$. Similarly Peters et al. (1995a) and Dillon (1982) find $L_{oz}/L_T \approx 0.8$, which (assuming $L_b \sim 1.6L_T$ as found in the former paper) gives a similar value. Baumert and Peters (2000) and Joseph et al. (2004), however, show a dependence of this ratio on the Richardson number. In the former they find $L_{oz}/L_b \approx 0.38\mathrm{Ri}^{-1/4}$ from the results of Rohr et al. (1988) giving $\varepsilon/QN \approx 0.29\mathrm{Ri}^{-1/2}$, though in the latter the dependence on Ri is less pronounced. These results imply that reasonable values for c_N and c_S are in the range 0.1–1.

5. Numerical results

a. Experimental setup

To compare with our parameterization and to assess what values of the parameters are appropriate, we conduct high-resolution numerical simulations of shear-driven stratified turbulence. The nonhydrostatic version of the MIT global circulation model (MITGCM; see Marshall et al. 1997) is used to model idealized shear and jet flows in a stratified environment. A 2.5 m × 2 m × 2 m box in x, y, and z is used that is cyclic in the x and y directions. Free-slip boundary conditions are imposed on the top and bottom boundaries to inhibit the generation of turbulence near the boundaries. The grid size is 2.083 mm in the x and y directions and varies in the z direction from 8.3 mm at the edges to 1.67 mm in the center of the domain. The constant background viscosity and diffusivity applied are $\kappa_o = 1.0 \times 10^{-6}\ \mathrm{m^2\ s^{-1}}$ and $\nu_o = 2.5 \times 10^{-6}\ \mathrm{m^2\ s^{-1}}$. Although these experiments are not strictly DNS (because they do not completely resolve the Kolmogorov scale) nor LES (because they do not use a subgrid-scale turbulence model), simulations were also conducted at a higher resolution (dx = 1.5625 mm) to check the statistical convergence of the solutions, both of which were found to have converged.

A linear equation of state is used with density solely dependent on temperature with an expansion coefficient of $2 \times 10^{-4}\ ^\circ\mathrm{C}^{-1}$. The initial stratification is constant ($N^2 = 0.0098$) and is due to a temperature difference across the channel of 10°C. The initial velocity profile is set for either a shear (with a velocity difference across the channel) given by

$$U(z) = U_o \tanh\left(\frac{z}{h_u}\right),$$

with $U_o = 0.0119\ \mathrm{m\ s^{-1}}$ and $h_u = 0.05$ m, or a jet (with a maximum velocity in the center of the channel) given by

$$U(z) = U_o \exp\left[-\left(\frac{z}{h_u}\right)^2\right],$$

where $U_o = 0.0261\ \mathrm{m\ s^{-1}}$ and $h_u = 0.084$ m. The model is forced by relaxation to the initial states in order that a statistically steady state can be reached, rather than run as a simple spindown case. This is important for diagnosing fluxes in a statistically steady state; in a spindown case the turbulence quickly decays as the Richardson number increases because of the mixing. The momentum forcing is constructed to force the horizontal-mean velocity profile in the x direction to evolve toward its initial profile $u_o(z)$. This is done using

$$\frac{\partial u}{\partial t} = \cdots + F_u + \lambda_u(u_o - \overline{u}), \quad \text{and}$$

$$\frac{\partial F_u}{\partial t} = \lambda_u^2(u_o - \overline{u}), \tag{16}$$

where $\overline{u}(z, t)$ is the u velocity averaged over the horizontal plane, and $\lambda_u = 0.01\ \mathrm{s^{-1}}$. Then in a statistically steady state the average velocity is the initial profile [the momentum forcing $F_u(z, t)$ has evolved from zero to match the momentum fluxes; see Hallberg and Gnanadesikan 2006]. This is done to ensure that our Richardson number stays low. Note that we are only forcing the average velocity profile rather than individual eddies. We cannot force the average tempera-

ture profiles in the same way since this can create spurious regions of convectively unstable stratification, so we relax to the initial temperature profile $T_o(z)$ with a relaxation time of 1000 s.

The jet and shear experiments spin up, developing KH billows which grow and eventually break into 3D turbulence. The turbulence and mean profiles gradually evolve until they reach a quasi-steady state where the forcing maintains the mean velocity and density profiles against the turbulent mixing. There is a slow drift due to the long-term evolution of the forcing profiles toward $\overline{u} = u_0$; however, the turbulence adjusts to a statistically steady state over a much shorter time scale. We define a quasi-steady state as that where the total TKE is in a statistically steady state for time scales greater than an overturning period (width of region/velocity scale ~10 s) and less than the forcing time scale [$\max(1/\lambda_U, 1/\lambda_T) = 1000$ s]. Profiles of velocity, temperature, TKE, and heat flux are calculated from these simulations by taking averages in x and y of quasi-steady quantities and then averaging over a period of 80 s. These profiles are provided to the parameterization in order to further constrain our parameters.

b. Results

Typical instantaneous slices in x and z of temperature during quasi-steady turbulent mixing are shown in Fig. 3 for the shear case and in Fig. 4 for the jet case. In the former the forced flow is from left to right at the top ($u > 0$) and from right to left at the bottom ($u < 0$), and in the latter there is a jet flowing from left to right in the center of the domain. Turbulent billows form over the regions of high shear, entraining fluid into the mixing region and reducing the stratification (see Figs. 3b and 4b). Eddy fluxes of temperature are shown in Figs. 3c and 4c and show the transport of temperature fluctuations due to eddies. Note that both positive and negative fluxes occur in individual eddies, although the average is negative. Also shown is the spanwise vorticity, which has filaments of large magnitude along fronts caused by high-velocity shear (Figs. 3d and 4d).

A bulk Reynolds number for the flow can be calculated using $\mathrm{Re}_b = \Delta U h/\nu$, where ν is the model viscosity and ΔU is the velocity difference across the mixing layer of width h. A local turbulent Reynolds number can also be defined using $\mathrm{Re} = Q^{1/2} L_b/\nu$. These give bulk Reynolds numbers of 3200 and 2400 for the shear and jet case respectively, and maximum Re values of 300 and 200, though these drop rapidly outside the mixing region. These are low values compared to estimated values in the oceans of $\mathrm{Re}_b \sim 10^7$ and $\mathrm{Re} \sim 10^4$; however, it is very difficult to achieve high Reynolds number flows in either numerical or laboratory experiments on this scale.

The exact terms in the horizontally averaged TKE budget can be calculated from

$$\frac{\partial \overline{Q}}{\partial t} + \frac{\partial F}{\partial z} = -\overline{u'w'}\,\overline{u}_z + \overline{w'b'} - \nu_o \overline{\nabla \mathbf{u}' . \nabla \mathbf{u}'}, \quad (17)$$

where $\overline{a}$ is the horizontally averaged part of the variable a and $a' = a - \overline{a}$ is the remainder. Also, $Q = (1/2)\mathbf{u}'.\mathbf{u}'$ is the TKE, and b is the buoyancy. The different terms are (from left to right) as follows: the tendency of horizontally averaged TKE; the vertical redistribution of TKE (due to eddy mixing, fluctuations of pressure ϕ, and viscous diffusion), where $F = \overline{w'Q'} + \overline{w'\phi'} + \nu_o \overline{Q}_z$; shear production of TKE; conversion of TKE into potential energy; and explicit gridscale dissipation. These terms, as calculated from the simulations, are time-averaged over the same periods as the profiles and plotted in Fig. 5 (except the tendency term, which is small). The error term is much smaller than the remaining terms, and mainly stems from numerical differences in the staggering of the pressure terms. These figures clearly show that TKE is being transferred vertically away from regions where it is produced (for example into the center of the jet in Fig. 5b). However, it is difficult to compare these terms from the simulation to those in our parameterization (11), since the TKE calculated from the simulations includes waves that may not contribute to mixing.

c. Comparison to parameterizations

Spatially averaged snapshots of various turbulent quantities are shown in Fig. 6 for the shear case and give an indication of the statistical steadiness of the solution. Profiles of background quantities u and T vary little in time whereas the turbulent quantities show some fluctuations, though no trend. In the center of the domain the shear is strong (Fig. 6c) and the Richardson number is low, reaching a minimum of 0.07 (Fig. 6e). The stratification has been weakened because of mixing in the central region, though the stratification on either side of the mixing region has increased due to conservation of mass. The turbulence generated by the shear-driven mixing can be seen in the TKE (Fig. 6f) and the temperature flux (Fig. 6g). The turbulent diffusivity, calculated as $\kappa = -(\overline{w'T'}/\overline{T}_z)$, is shown in Fig. 6h and, as expected, is large over the region where Ri is small.

Figure 7 shows the time-averaged profiles from the shear case with our parameterizations for three sets of parameters. The functions $F(\mathrm{Ri})$ are shown in Fig. 7b with all parameters listed in Table 2. These parameters

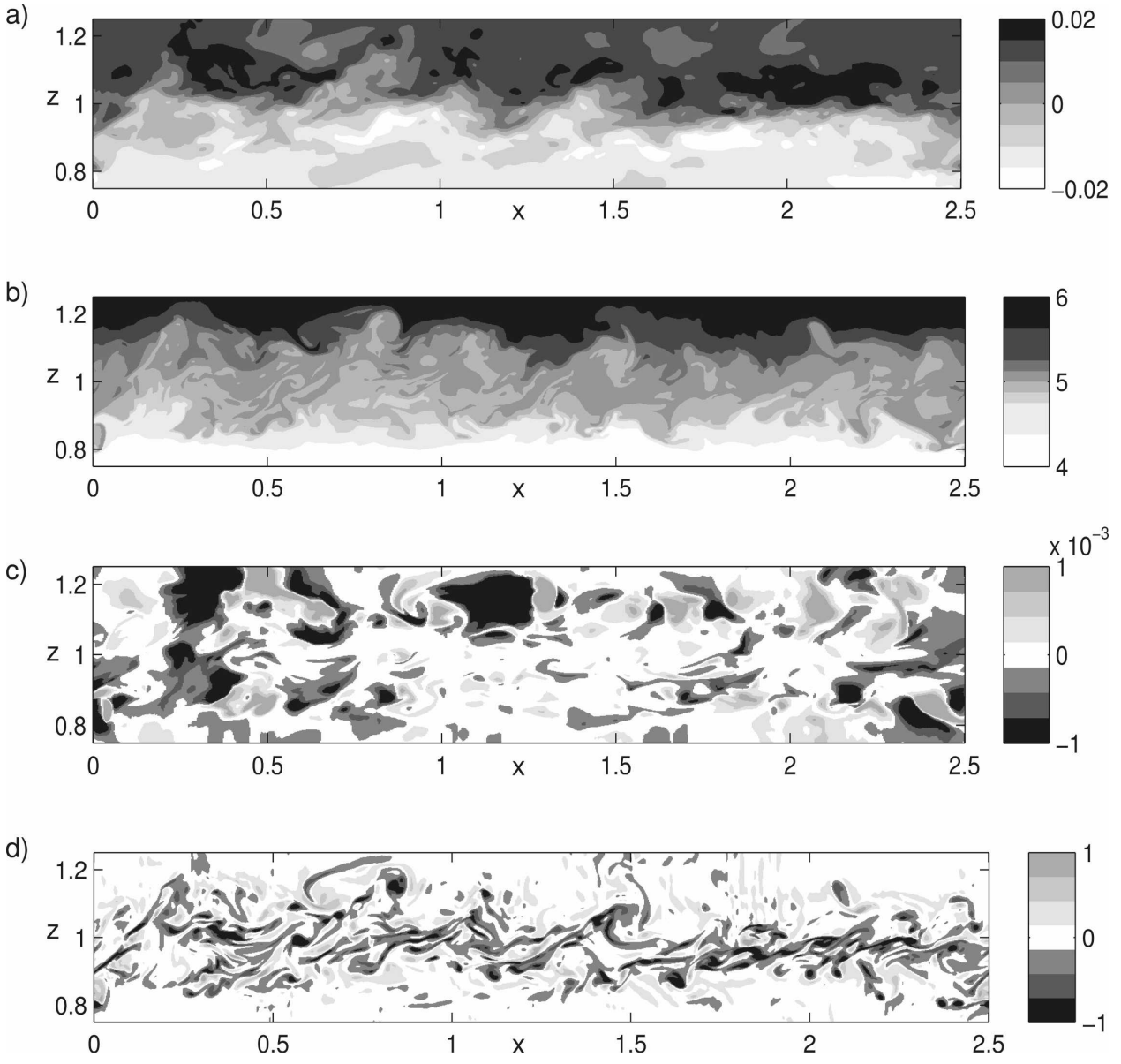

FIG. 3. Instantaneous slices for the shear case showing (a) velocity u (m s^{-1}) in the x direction, (b) temperature (°C), (c) eddy temperature flux $W'T'$ (°C m s^{-1}), where $A' = A - \overline{A}$ and $\overline{A}$ is the average of the profile A in x, y and t, and (d) spanwise vorticity (s^{-1}).

have been chosen to minimize the difference of the predicted eddy diffusivity (calculated using profiles of N and S from the model results) from that calculated in the model for both the shear and jet cases, given a value of Ri_c of 0.25, 0.3, or 0.35. Each of these sets produces essentially the same parameterization (shown in a dashed line in Figs. 7c and 7d) which matches the diffusivity (solid line) very well and the buoyancy flux reasonably well. The discrepancies in the buoyancy flux are due to larger fluxes than predicted between z = 0.7–0.85 m and z = 1.15–1.3 m. The dotted line shows the predicted diffusivity and flux for the original TP, in which the diffusivity is zero for $\mathrm{Ri} \geq 0.8$. This can predict the location of the enhanced mixing, although it does not capture the magnitude or the width of the mixing.

The profiles for the jet case are shown in Fig. 8. The main difference with the previous case is the presence of two regions of high shear (Fig. 8c), which in turn create two regions of low Richardson number. However, because the large-scale shear in the center of the jet, is small, the Richardson number is large. The tur-

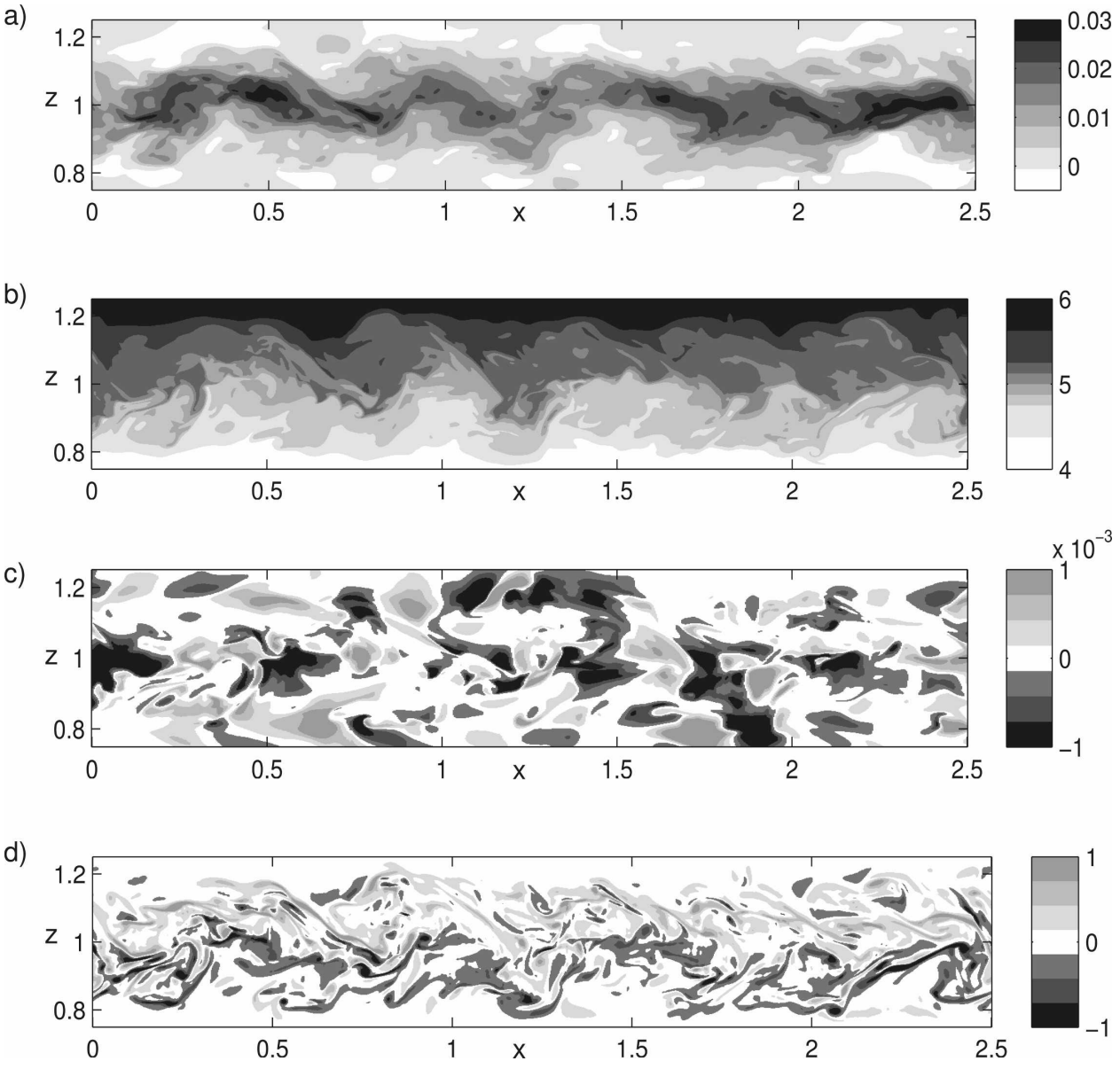

FIG. 4. As in Fig. 3, but for the jet case.

bulent eddy diffusivity has two peaks where the Richardson number is small, but the diffusivity is nonzero in the center of the jet, contrary to predictions based on local values of the Richardson number. This result is also seen in Joseph et al. (2004), who also find very different local scaling laws of κ with Ri for the inner and outer regions of the diffusivity. Using the same parameterizations as for the shear case, we can capture the shape and magnitude of the diffusivity and buoyancy fluxes (Figs. 9c and 9d). The previous TP parameterization gives zero eddy diffusivity, and therefore zero buoyancy flux, in the center of the jet where the Richardson number is large. Any local parameterization [such as the interior part of KPP or Pacanowski and Philander (1981)] that assumes a small diffusivity where Ri is large would suffer from this problem. Although it has been shown that the magnitude of the mixing is less important than the critical Ri where mixing stops, a local parameterization would imply no mixing across the center of the jet, creating a nonphysical mixing barrier.

It is clear that these three parameter sets produce very similar results. Indeed, it appears that the important aspect of $F(\mathrm{Ri})$ is in capturing the value for the minimum Richardson number of the profile. The parameter sets differ mainly in the critical value of Ri:

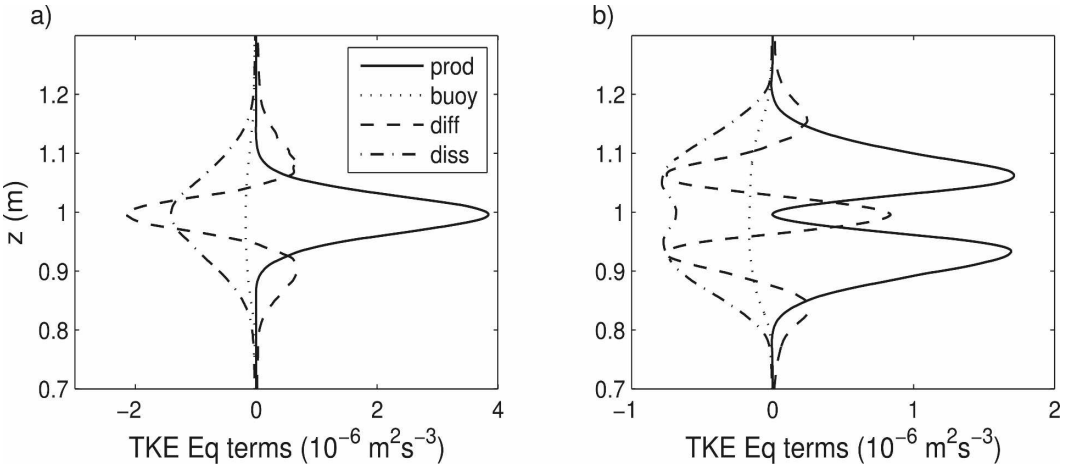

FIG. 5. Terms from the TKE balance (17) calculated explicitly from the simulations and averaged horizontally and temporally for (a) the shear case and (b) the jet case. The shear production of TKE (solid line) is redistributed by a diffusion term (dashed), and transferred to potential energy through a buoyancy term (dotted) or dissipated (dashed–dotted).

while this seems to be less important for these profiles (probably because Ri varies rapidly in z), nonetheless it is extremely important in governing how much mixing occurs in an evolving flow (Xu et al. 2006; Papadakis et al. 2003).

d. Comparison to two equation turbulence models

Although no local Richardson number parameterization can reproduce the buoyancy flux across the jet, there are more complex nonlocal parameterizations also in use. These are two equation turbulence models such as the k–ε model (see Marchuk et al. 1977; Rodi 1987; Burchard and Baumert 1995), which consists of equations for the TKE Q and dissipation ε:

$$\frac{\partial Q}{\partial t} = \frac{\partial}{\partial z}\left(\frac{\nu}{\sigma_\kappa}\frac{\partial Q}{\partial z}\right) + \nu S^2 - \kappa N^2 - \varepsilon, \quad \text{and}$$

$$\frac{\partial \varepsilon}{\partial t} = \frac{\partial}{\partial z}\left(\frac{\nu}{\sigma_\varepsilon}\frac{\partial \varepsilon}{\partial z}\right) + \frac{\varepsilon}{Q}(c_1 \nu S^2 - c_3 \kappa N^2 - c_2 \varepsilon) \quad (18)$$

for given parameters σ_k, σ_ε, c_1, c_2, and c_3. Note that we have used the notation of Q for the TKE to be consistent with the rest of this paper, rather than the more commonly used k. The turbulent eddy viscosity and diffusivity are calculated from

$$\nu = c_\mu \frac{Q^2}{\varepsilon}, \quad \text{and}$$

$$\kappa = c'_\mu \frac{Q^2}{\varepsilon}. \quad (19)$$

The stability functions c_μ and c'_μ are functions of NQ/ε and SQ/ε and are generally nonlinear relationships derived from balances between velocity and temperature correlations.

The Mellor–Yamada level 2.5 model (Mellor and Yamada 1982; Galperin et al. 1988) has a similar structure except that it uses an evolution equation for Ql (where l is the length scale $l = Q^{3/2}/\varepsilon$) instead of the turbulent dissipation in (18). An important difference is the inclusion of a wall function in c_2 that is dependent upon the distance from the wall and is used to capture the length scale for boundary layer turbulence.

To compare these models to our results we use the turbulence module from the General Ocean Turbulence Model (GOTM; see Umlauf et al. 2005). We use the GOTM implementations of the k–ε model (Umlauf and Burchard 2005; Rodi 1987) and the Mellor–Yamada model (see also Mellor and Yamada 1982) with parameters taken from these papers. The steady-state Richardson numbers of the k–ε model and the Mellor–Yamada model are 0.25 and 0.18 respectively, and the Mellor–Yamada model uses the length scale clipping from Galperin et al. 1988. For the Mellor–Yamada model we use the stability function of Kantha and Clayson (1994), and for the k–ε model that of Canuto et al. (2001). By using the velocity and density profiles from our MITGCM results and keeping these fixed, we find the profiles of turbulent diffusivity predicted by both models when a steady state is reached.

Results from these models are compared to diffusivities and buoyancy fluxes for the shear and jet cases in Fig. (10). Also plotted is the new parameterization p_1. The k–ε model does a good job of capturing the width and magnitude of the mixing, which is particularly impressive since it has not been tuned for this data; how-

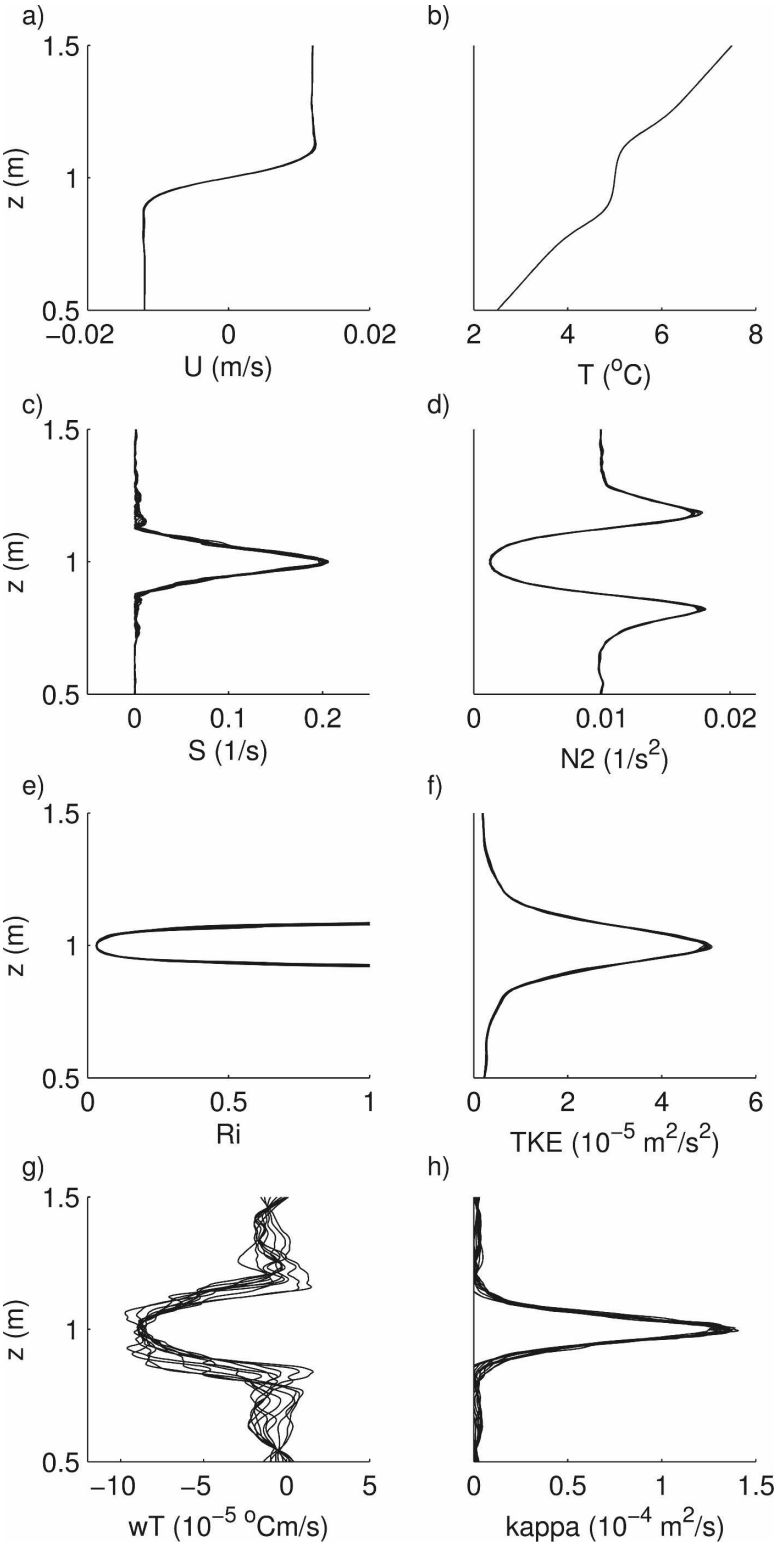

FIG. 6. Horizontally averaged snapshots of MITGCM results during the quasi-steady state in the shear case. Profiles shown are of (a) horizontal velocity (m s^{-1}), (b) temperature (°C), (c) velocity shear (s^{-1}), (d) buoyancy frequency (s^{-2}), (e) Richardson number, (f) TKE (m^2 s^{-2}), (g) temperature flux ($\overline{w'T'}$) (°C m s^{-1}), and (h) turbulent diffusivity κ (m^2 s^{-1}).

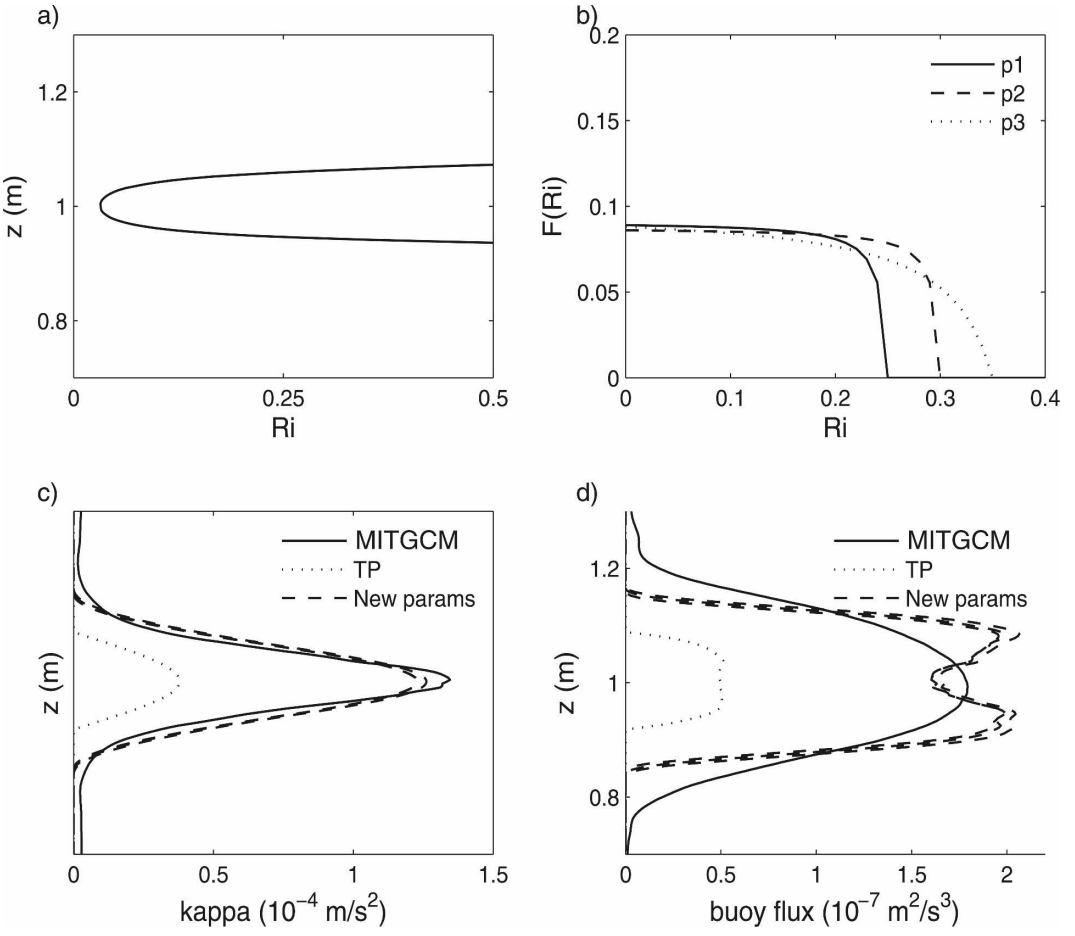

FIG. 7. Comparison of eddy diffusivities and fluxes from MITGCM results and our parameterization for the shear case. (a) Vertical profile of Ri based on the time and horizontal averages of N and S; (b) three functions F(Ri) used in parameterizations p1, p2, and p3; (c) vertical profile of the turbulent diffusivity κ from the time and horizontal average of the MITGCM results (solid line), predicted diffusivity from our parameterizations p1, p2, and p3 (dashed lines), and the predicted diffusivity from TP (dotted line); and (d) as in (c) but for the buoyancy fluxes.

ever, the Mellor–Yamada model does less well, overestimating the mixing in the shear layer and underestimating it in the jet. The difference between the two models does not seem to stem from the different values of Ri_s or the length clipping.

The success of the k–ε model suggests that good results may be obtained using this parameterization, but in order to be incorporated into a large-scale ocean and climate model it must be able to deal with long time steps. Our new parameterization is simple enough to be able to treat mixing implicitly, including the effects of the mixing on the ambient velocity and density profiles.

TABLE 2. Parameter sets used.

Parameter set	F_o	Ri_c	α	λ	c_N	c_S
p_1	0.089	0.25	−0.97	0.82	0.24	0.14
p_2	0.085	0.30	−0.94	0.86	0.26	0.13
p_3	0.088	0.35	−0.89	0.81	0.28	0.12

6. Discussion of implementation in ocean climate models

To apply this parameterization to coarse-resolution ocean climate models we need sufficient resolution to resolve the mixing layers. Data from field experiments (see Peters and Johns 2005; Peters et al. 1995b) suggest a value of $L_b = O(1\text{–}10)$ m and mixing layer widths of 50–150 m (though regions where Ri is less than a critical value can be much narrower). The buoyancy length scale may not be fully resolved in the EUC of ocean climate models, but is resolvable in overflows with isopycnal coordinates where the resolution is naturally

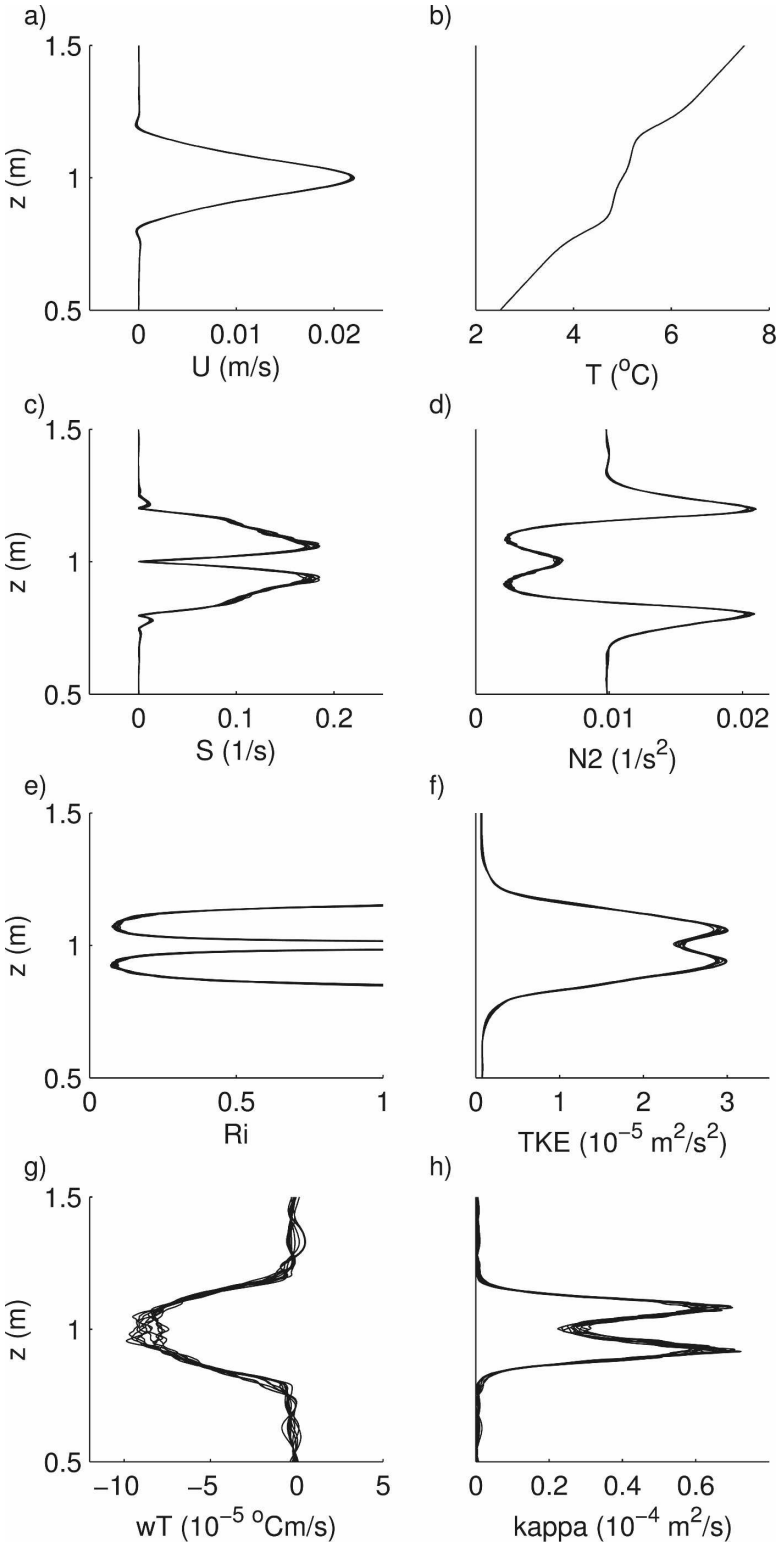

FIG. 8. As in Fig. 6, but for the jet case.

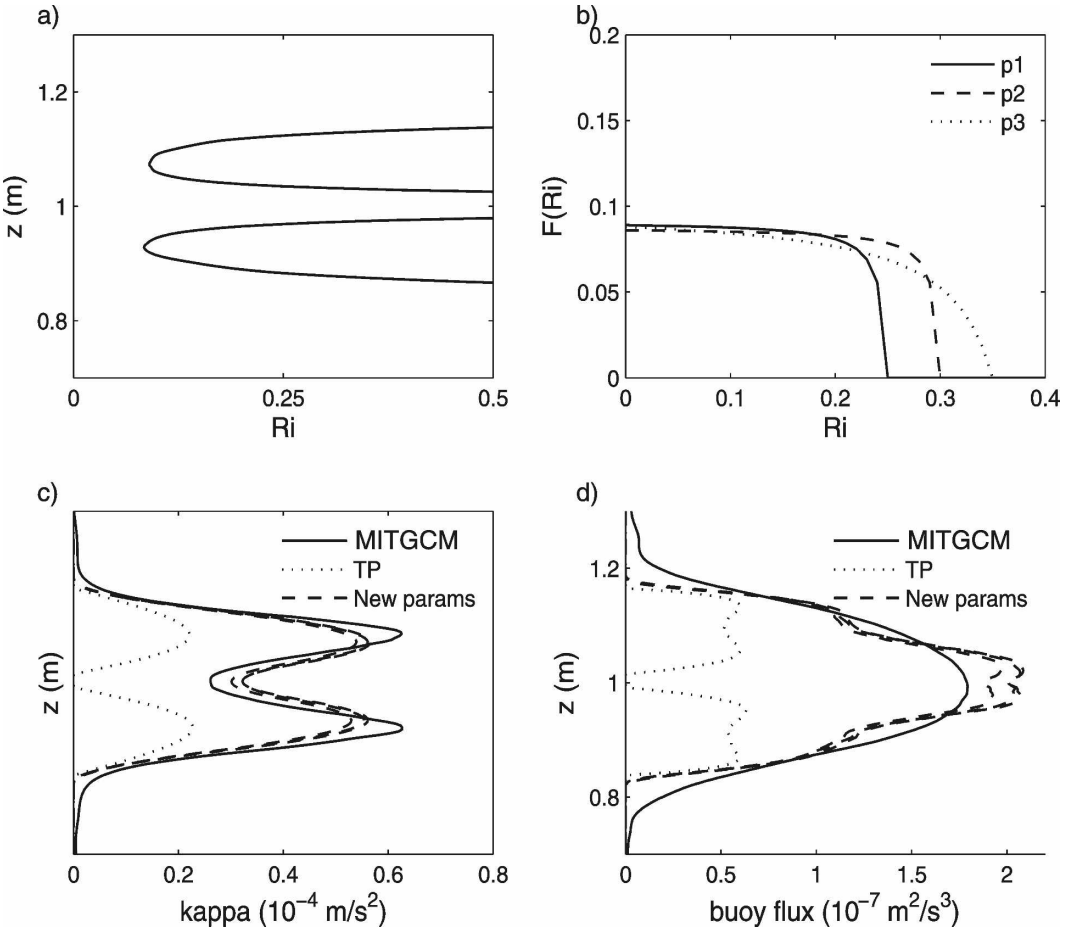

FIG. 9. As in Fig. 7, but for the jet case.

concentrated at regions of high stratification. For z-coordinate models of overflows, the simulation of mixing is currently limited by the *horizontal* resolution, which must be able to resolve the bottom boundary layer thickness divided by the topographical slope to avoid excessive numerical mixing (Winton et al. 1998). If the buoyancy length scale is not resolved then our parameterization approximates to $\kappa = 2SFL_d^2$. This is a local balance where $\kappa = 0$ when $S = 0$; however, we would not expect the mixing to significantly penetrate to neighboring grid cells when then grid size is larger than L_d, so this numerical approximation is benign and is resolution independent.

One possible issue of applying this parameterization to a coarse-resolution model is the sensitivity of the Richardson number, and hence the mixing, on the resolution. To investigate this issue we sampled our averaged profiles of velocity, temperature, and buoyancy flux from our model data at different vertical resolutions and applied our parameterizations to these sampled profiles. Figure 11 shows the results for the shear and jet cases with vertical resolutions of 0.1, 0.067, 0.04, and 0.002 m with approximately 2, 3–4, 4–6, and 100 points across the low Richardson number region respectively. For a shear or jet in the ocean with a total mixing width of 100 m, these resolutions scale to approximately 50, 33, 20, and 1 m respectively. Our parameterization p_3 produces diffusivities that vary little as the resolution becomes coarser (middle panels). For the coarsest resolution (dashed line), the predicted turbulent diffusivity does about as well as the diffusivity from the model (calculated from the sampled buoyancy flux and temperature). Obviously, these results depend on sampling at very low resolutions; the process of staggering, which ensures a point at the center of the low Richardson number regions, gives better results. These results suggest that our parameterization needs only a few points across the mixing region to give plausible results.

To be incorporated into a large-scale ocean climate model, any parameterization must be able to deal with time steps that are long compared to both the time scale

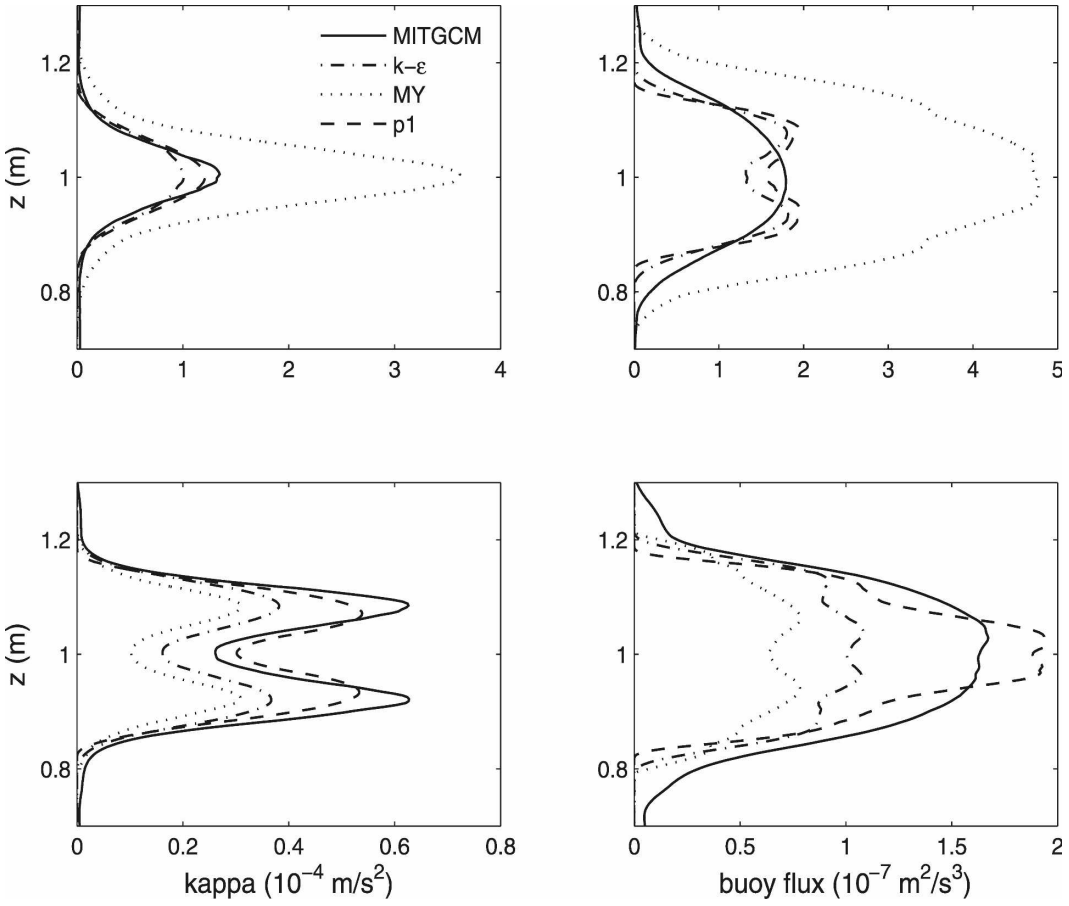

FIG. 10. Comparisons of (left) turbulent eddy diffusivity and (right) buoyancy flux from our new parameterization p1 (dashed) with the Mellor–Yamada parameterization (dotted), the κ–ε parameterization (dashed–dotted) and the MITGCM results (solid). (top) Results from the shear case and (bottom) those from the jet case.

on which the turbulence evolves and the time scale on which it alters the large-scale flow. To do this it should treat the mixing implicitly, including the negative feedback from the modification of the resolved flow and density structure by the mixing within each time step. Our parameterization is simple enough to be implemented implicitly, including this negative feedback, and since we are solving directly for κ, it gives a robust numerical solution with just a few iterations.

7. Conclusions

We have presented a theory for parameterizing shear-driven turbulent mixing that is simple enough to be used for climate modeling. This parameterization does not rely on dimensional constants, so it should be relevant for shear-driven mixing in both overflows and the EUC. It also combines two length scales: the width of the low Richardson number region and the buoyancy length scale (the length scale over which turbulence decays because of stratification). This creates a nonlocal parameterization that allows a vertical transport of turbulence from regions with a low Richardson number to the surrounding areas over the buoyancy length scale. Our numerical results show that this is an important physical process in mixing across a jet that is missing from parameterizations based on the local Richardson number. It also has the benefit of providing a spatially and temporally smooth eddy diffusivity, which is particularly hard to achieve with local parameterizations when the Richardson number profile is noisy.

The aim of our parameterization is to model the shear-driven mixing in regions where it is important for the climate (overflows and the EUC), while remaining simple enough to be implemented implicitly. Implicit solutions of the turbulent mixing are critical for applying a scheme to climate regions where time steps are large, or to isopycnal models where layer thicknesses can be small. Existing parameterizations are specific to the Pacific EUC (the interior part of KPP) or are more sophisticated general turbulence models (k–ε) used in regional models. Our new parameterization is simple

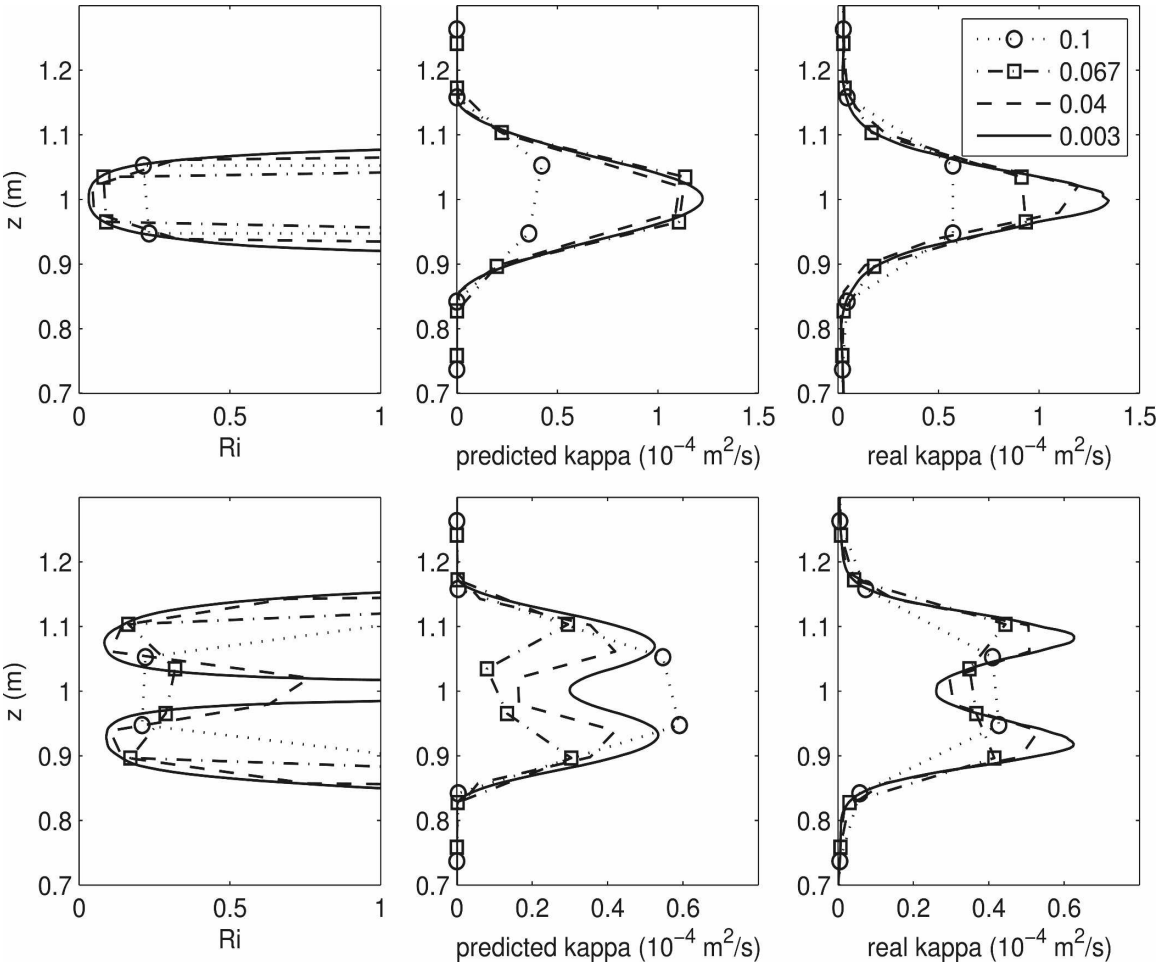

FIG. 11. The (left) Richardson number, (middle) the diffusivity predicted by the parameterization, and (right) the diffusivity calculated from the model flux for different vertical resolutions. (top) Shear case and (bottom) jet case. The vertical resolutions are 0.003 (solid), 0.04 (dashed), 0.067 (dashed–dotted with square markers), and 0.1 m (dotted with circular markers).

enough to be able to treat mixing implicitly as in Hallberg (2000) and is also better physically motivated.

We have examined various limits of our parameterization and found good agreement with existing work. Our numerical results with shear and jet profiles support our theory and have provided parameter values that are consistent with ranges from previous work.

Our parameterization has been implemented in the Hallberg Isopycnal Model for use in coupled climate simulations. It has proved to be robust and efficient, and initial results from climate simulations have been encouraging. A follow-up paper describing the numerical implementation and results is planned.

Acknowledgments. The authors thank Hartmut Peters, Anand Gnanadesikan, Lars Umlauf, George Nurser, and members of the Gravity Current Entrainment Climate Process Team for useful discussions and suggestions. Comments from anonymous reviewers helped to substantially improve this manuscript. This work was supported by the Gravity Current Entrainment Climate Process Team, funded through NOAA and NSF.

APPENDIX

Idealized Solutions

To illustrate our parameterization we can find analytical solutions for the turbulent diffusivity given simplified profiles. In particular we consider the situation where the source $G = 2SF(\mathrm{Ri})$ and the decay length scale L_d are constant over the mixing region $|z| \leq d$. Outside this region we assume that the turbulence decays away infinitely quickly so that $\kappa = 0$. Within the mixing region our parameterization is then

$$\frac{\partial^2 \kappa}{\partial z^2} - \frac{\kappa}{L_d^2} = -G, \tag{A1}$$

which has the solution

$$\kappa = GL_d^2\left(1 - \frac{\cosh\gamma Z}{\cosh\gamma}\right), \tag{A2}$$

where $\gamma = d/L_d$ and $Z = z/d$ (with $|Z| \le 1$). Then if the decay length scale [or buoyancy length scale since $\lambda \sim O(1)$] is much less then the width of the low Richardson number region (e.g., the TKE is small), we have $\gamma \gg 1$, which gives

$$\kappa \sim GL_d^2[1 - e^{-\gamma(1-|Z|)}]. \tag{A3}$$

Then the maximum value of κ scales with GL_d^2. Indeed, this scaling holds throughout the layer, except in a narrow boundary layer of width $1/\gamma$ near the edges, where the diffusivity decreases to zero.

In the opposite limit (of large TKE) then $\gamma \ll 1$ and the solution becomes

$$\kappa \sim GL_d^2\left[\frac{\gamma^2}{2}(1 - Z^2)\right]$$

$$= \frac{Gd^2}{2}(1 - Z^2). \tag{A4}$$

Then the turbulent diffusivity is parabolic with a maximum value of $Gd^2/2$. Hence the maximum diffusivity scales with the square of the minimum of the buoyancy length scale and the width of the low Ri layer, though the width of the diffusivity always spans the mixing region.

This analysis has assumed that outside the mixing region the decay length scale $L_d = 0$. With a nonzero value due to the vertical transport of TKE outside the mixing region we have $\kappa \propto e^{-z/L_d}$ (for $z > 0$). Hence the turbulent mixing decays away exponentially from the mixing region.

REFERENCES

Abarbanel, H. D. I., D. D. Holm, J. E. Marsden, and T. S. Ratiu, 1986: Nonlinear stability analysis of stratified fluid equilibria. *Philos. Trans. Roy. Soc. London,* **318A,** 349–409.

Baumert, H., and H. Peters, 2000: Second-moment closures and length scales for weakly stratified turbulent shear flows. *J. Geophys. Res.,* **105,** 6453–6468.

Burchard, H., and H. Baumert, 1995: On the performance of a mixed layer model based on the *k*–ε turbulence closure. *J. Geophys. Res.,* **100,** 8523–8540.

——, E. Deleersnijder, and G. Stoyan, 2005: Some numerical aspects of turbulence-closure models. *Marine Turbulence: Theories, Observations, and Models,* H. Baumert, J. Simpson, and J. Sünderman, Eds., Cambridge University Press, 202–206.

Canuto, V. M., A. Howard, Y. Cheng, and M. S. Dubovikov, 2001: Ocean turbulence. Part I: One-point closure model—Momentum and heat vertical diffusivities. *J. Phys. Oceanogr.,* **31,** 1413–1426.

Chang, Y. S., X. Xu, T. Özgökmen, E. P. Chassignet, H. Peters, and P. F. Fischer, 2005: Comparison of gravity current mixing parameterizations and calibration using a high-resolution 3D nonhydrostatic spectral element model. *Ocean Modell.,* **10,** 342–368.

De Silva, I. P. D., A. Brandt, L. J. Montenegro, and H. J. S. Fernando, 1999: Gradient Richardson number measurements in a stratified shear layer. *Dyn. Atmos. Oceans,* **30,** 47–63.

Dillon, T. M., 1982: Vertical overturns: A comparison of Thorpe and Ozmidov length scales. *J. Geophys. Res.,* **87,** 9601–9613.

Ellison, T. H., and J. S. Turner, 1959: Turbulent entrainment in stratified flows. *J. Fluid Mech.,* **6,** 423–448.

Galperin, B., L. H. Kantha, S. Hassid, and A. Rosati, 1988: A quasi-equilibrium turbulent energy model for geophysical flows. *J. Atmos. Sci.,* **45,** 55–62.

Hallberg, R., 2000: Time integration of diapycnal diffusion and Richardson number–dependent mixing in isopycnal coordinate ocean models. *Mon. Wea. Rev.,* **128,** 1402–1419.

——, and A. Gnanadesikan, 2006: The role of eddies in determining the structure and response of the wind-driven Southern Hemisphere overturning: Results from the modeling eddies in the Southern Ocean project. *J. Phys. Oceanogr.,* **36,** 2232–2252.

Joseph, B., A. Mahalov, B. Nicolaenko, and K. L. Tse, 2004: Variability of turbulence and its outer scales in a model tropopause jet. *J. Atmos. Sci.,* **61,** 621–643.

Kantha, L. H., and C. A. Clayson, 1994: An improved mixed layer model for geophysical applications. *J. Geophys. Res.,* **99,** 25 235–25 266.

Koop, C., and F. Browand, 1979: Instability and turbulence in a stratified layer with shear. *J. Fluid Mech.,* **93,** 135–159.

Large, W. G., J. C. McWilliams, and S. C. Doney, 1994: Oceanic vertical mixing: A review and a model with a nonlocal boundary layer parameterization. *Rev. Geophys.,* **32,** 363–403.

Legg, S., R. W. Hallberg, and J. B. Girton, 2006: Comparison of entrainment in overflows simulated by z-coordinate, isopycnal, and non-hydrostatic models. *Ocean Modell.,* **11,** 69–97.

Lesieur, M., 1997: *Turbulence in Fluids.* 3rd ed. Kluwer, 515 pp.

Marchuk, G. I., V. P. Kochergin, V. I. Klimok, and V. A. Sukhorukov, 1977: On the dynamics of the ocean surface mixed layer. *J. Phys. Oceanogr.,* **7,** 865–875.

Marshall, J., A. Adcroft, C. Hill, L. Perelman, and C. Heisey, 1997: A finite-volume, incompressible Navier Stokes model for studies of the ocean on parallel computers. *J. Geophys. Res.,* **102,** 5753–5766.

McDougall, T., and W. Dewar, 1998: Vertical mixing and cabbeling in layered models. *J. Phys. Oceanogr.,* **28,** 1458–1480.

Mellor, G. L., and T. Yamada, 1982: Development of a turbulence closure model for geophysical fluid problems. *Rev. Geophys.,* **20,** 851–875.

Miles, J., 1961: On the stability of heterogeneous shear flows. *J. Fluid Mech.,* **10,** 496–508.

Moin, P., and J. Kim, 1982: Numerical investigation of turbulent channel flow. *J. Fluid Mech.,* **118,** 341–377.

Moum, J. N., 1996: Energy-containing scales of turbulence in the ocean thermocline. *J. Geophys. Res.,* **101,** 14 095–14 109.

Pacanowski, R. C., and S. G. H. Philander, 1981: Parameterization of vertical mixing in numerical models of tropical oceans. *J. Phys. Oceanogr.,* **11,** 1443–1451.

Papadakis, M., E. Chassignet, and R. W. Hallberg, 2003: Numeri-

cal simulations of the Mediterranean sea outflow: Impact of the entrainment parameterization in an isopycnic coordinate ocean model. *Ocean Modell.,* **5,** 325–356.

Peters, H., and W. E. Johns, 2005: Mixing and entrainment in the Red Sea outflow plume. Part II: Turbulence characteristics. *J. Phys. Oceanogr.,* **35,** 584–600.

——, M. C. Gregg, and T. B. Sanford, 1995a: Detail and scaling of turbulent overturns in the Pacific Equatorial Undercurrent. *J. Geophys. Res.,* **100,** 18 349–18 368.

——, ——, and ——, 1995b: On the parameterization of equatorial turbulence—Effect of fine-scale variations below the range of the diurnal cycle. *J. Geophys. Res.,* **100** (C9), 18 333–18 348.

Rodi, W., 1987: Examples of calculation methods for flow and mixing in stratified flows. *J. Geophys. Res.,* **92,** 5305–5328.

Rohr, J. J., E. C. Itsweire, K. N. Helland, and C. W. Van Atta, 1988: Growth and decay of turbulence in a stably stratified shear flow. *J. Fluid Mech.,* **195,** 77–111.

Shih, L. C., J. R. Koseff, J. H. Ferziger, and C. R. Rehmann, 2000: Scaling and parameterization of stratified homogeneous turbulent shear flow. *J. Fluid Mech.,* **412,** 1–20.

Smyth, W. D., and J. N. Moum, 2000: Length scales of turbulence in stably stratified mixing layers. *Phys. Fluids,* **12,** 1327–1342.

Strang, E. J., and H. J. S. Fernando, 2001: Entrainment and mixing in stratified shear flows. *J. Fluid Mech.,* **428,** 349–386.

Tse, K. L., A. Mahalov, B. Nicolaenko, and H. J. S. Fernando, 2003: Quasi-equilibrium dynamics of shear-stratified turbulence in a model tropospheric jet. *J. Fluid Mech.,* **496,** 73–103.

Turner, J., 1986: Turbulent entrainment: The development of the entrainment assumption and its application to geophysical flows. *J. Fluid Mech.,* **173,** 431–471.

Umlauf, L., and H. Burchard, 2005: Second-order turbulence closure models for geophysical boundary layers. A review of recent work. *Cont. Shelf Res.,* **25,** 795–827.

——, ——, and K. Hutter, 2003: Extending the k-ω turbulence model towards oceanic applications. *Ocean Modell.,* **5,** 195–218.

——, —— and K. Bolding, cited 2005: GOTM: Sourcecode and test case documentation, version 3.2. [Available online at http://www.gotm.net/pages/documentation/manual/html/.]

Winton, M., R. Hallberg, and A. Gnanadesikan, 1998: Simulation of density-driven frictional downslope flow in z-coordinate ocean models. *J. Phys. Oceanogr.,* **28,** 2163–2174.

Xu, X., Y. S. Chang, H. Peters, T. M. Özgökmen, and E. P. Chassignet, 2006: Parameterization of gravity current entrainment for ocean circulation models using a high-order 3D nonhydrostatic spectral element model. *Ocean Modell.,* **14,** 19–44.

Yu, Z. J., and P. S. Schopf, 1997: Vertical eddy mixing in the tropical upper ocean: Its influence on zonal currents. *J. Phys. Oceanogr.,* **27,** 1447–1458.